

Article

Application of a Modified Differential Quadrature Finite Element Method to Flexural Vibrations of Composite Laminates with Arbitrary Elastic Boundaries

Wei Xiang , Xin Li and Lina He

School of Mechanical Engineering, Southwest Jiaotong University, Chengdu 610031, China

* Correspondence: xiangwei@swjtu.edu.cn

Abstract: This paper formulates a modified differential quadrature finite element method (DQFEM) by a combination of the standard DQFEM and the virtual boundary spring technique, which makes it easy to implement arbitrary elastic restraints by assigning reasonable values to the boundary spring stiffnesses. This new formulated method can offer a unified solution for flexural vibrations of composite laminates subjected to general elastic boundary combinations including all the classical cases. The influences of the number of Gauss–Lobatto nodes and the boundary spring stiffnesses on the convergence characteristics of natural frequencies are investigated, and some conclusions are drawn in terms of the minimum number of unilateral nodes required to generate convergent solutions and the optimal values of the boundary spring stiffnesses to simulate classical boundaries. Numerical examples are performed for composite laminates under various classical boundary conditions. Excellent accuracy, numerical stability, and reliability of the present method are demonstrated by comparisons with available exact and numerical solutions in open literatures. Additionally, for elastically constrained composite laminates, which are beyond the scope of most existing approaches, numerous new results obtained by the present method may serve as reference values for other research.



Citation: Xiang, W.; Li, X.; He, L. Application of a Modified Differential Quadrature Finite Element Method to Flexural Vibrations of Composite Laminates with Arbitrary Elastic Boundaries. *Buildings* **2022**, *12*, 1380. <https://doi.org/10.3390/buildings12091380>

Academic Editors: Zechuan Yu and Dongming Li

Received: 12 August 2022

Accepted: 1 September 2022

Published: 4 September 2022

Publisher's Note: MDPI stays neutral with regard to jurisdictional claims in published maps and institutional affiliations.



Copyright: © 2022 by the authors. Licensee MDPI, Basel, Switzerland. This article is an open access article distributed under the terms and conditions of the Creative Commons Attribution (CC BY) license (<https://creativecommons.org/licenses/by/4.0/>).

Keywords: differential quadrature finite element method (DQFEM); virtual boundary spring; composite laminates; arbitrary elastic boundary; flexural vibration

1. Introduction

Composite laminates are increasingly used in various engineering structures, such as space vehicles, aircraft, naval ships, and submarines, which are usually subjected to frequent dynamic loads. Hence, a thorough understanding of the vibration characteristics of laminates is critical for the design and analysis of composite structures.

In the past few years, many efforts have been devoted to developing accurate and efficient methods to determine the vibration behaviors of composite laminates. A comprehensive review of the recent works on this subject has been provided by Sayyad and Ghugal [1], covering both analytical and numerical methods. By contrast with analytical methods known to be limited to only a few cases, numerical methods are more effective in a wide range of cases involving various physical properties, arbitrary boundary conditions, and sophisticated loading configurations. Various numerical procedures are available for flexural vibrations of multi-layered composite plates [2–12], among which the most representative and widely used one is the finite element method (FEM) that has already been successfully incorporated into commercial software. However, FEM generally uses low-order approximating functions; consequently, a higher accuracy can only be achieved by mesh refinement, resulting in a higher computation cost. To tackle this problem, more intensive research activities are motivated, focusing on high-order schemes such as the mesh-free method [13,14] and differential quadrature (DQ) method [15,16], which tend to yield highly accurate solutions with far fewer degrees of freedom (DOFs) than low-order ones owing to the use of high-order basis functions.

Although increased interest is still in the extension of various numerical methods to the vibration analysis of composite laminates, most of the previous research was confined to the classical boundary conditions comprised of simply supported, clamped, and free boundaries. However, the boundary conditions of numerous engineering structures might not always be ideal essentially. Actually, elastic supports are more commonly seen in practice, and a relative lack of corresponding research still exists.

Motivated by the state-of-the-art, this paper aims to seek for an accurate, efficient, and reliable method for the flexural vibration analysis of composite laminates subjected to arbitrary elastic boundaries. The current work draws on the idea of a well-established high-order scheme referred to as the differential quadrature finite element method (DQFEM) [17,18], in which the DQ rule and the Gauss–Lobatto integration rule are utilized to discretize the energy functional of structures. Fast convergence, high precision, and efficiency, as well as remarkable versatility of the DQFEM, have been validated in the previous research [17,18]. The boundary conditions in both DQFEM and the standard FEM are implemented via the same way, that is, the elimination method. However, this classical approach is only limited to dealing with the classical boundaries but is unable to process general elastic boundaries.

On the purpose of extending the applicability of DQFEM to elastically restrained composite structures, a modified DQFEM is proposed by introducing the virtual boundary spring technique [19–28], in which general elastic restraints including several classical boundary conditions can be easily realized by assigning reasonable values to the virtual boundary spring stiffnesses.

It is well-known that equivalent single-layer laminate theories, which treat a laminated plate as an equivalent homogeneous and orthotropic single layer, are adequate to predict the global response behaviors of composite laminates. Therefore, in the present paper, the widely acknowledged first-order shear deformation theory (FSDT) [29,30] is adopted to model the flexural vibration behavior of composite laminates, since it affords the best compromise between accuracy and efficiency. A detailed formulation of this modified DQFEM is presented for flexural vibrations of rectangular laminates with general elastic restraints. Numerical examples are carried out to discuss the convergence characteristics and validate the accuracy of the present approach.

2. Modified DQFEM Formulation for Composite Laminates

2.1. Constitutive Relations for Composite Laminate

Figure 1 schematically shows a rectangular composite laminate (length a , width b , and thickness h) composed of multiple orthotropic layers with the same thickness and material properties. The xy plane of the Cartesian coordinate system is located on the mid-plane of the laminate, with the origin placed at one corner.

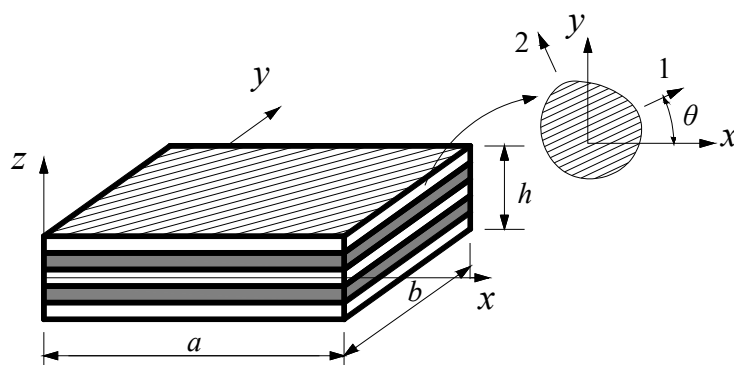


Figure 1. Schematic representation of a composite laminate.

Each single-layer of the laminate is usually assumed to be in the plane-stress state. As shown in Figure 2, σ_1 and σ_2 are the normal stress components in the principle directions of the single-layer, and τ_{12} represents the shear stress component. The constitutive

equations relating in-plane stresses and strains for each layer are expressed in the material coordinate system as

$$\begin{bmatrix} \sigma_1 \\ \sigma_2 \\ \tau_{12} \end{bmatrix} = \begin{bmatrix} Q_{11} & Q_{12} & 0 \\ Q_{12} & Q_{22} & 0 \\ 0 & 0 & Q_{66} \end{bmatrix} \begin{bmatrix} \varepsilon_1 \\ \varepsilon_2 \\ \gamma_{12} \end{bmatrix}, \begin{bmatrix} \tau_{13} \\ \tau_{23} \end{bmatrix} = \begin{bmatrix} Q_{44} & 0 \\ 0 & Q_{55} \end{bmatrix} \begin{bmatrix} \gamma_{13} \\ \gamma_{23} \end{bmatrix}, \quad (1)$$

in which ε_i ($i = 1, 2$) and γ_{ij} ($i, j = 1, 2, 3$) are strain components; Q_{ij} are modulus components with respect to the material coordinate system in the following form:

$$Q_{11} = E_1 / (1 - \nu_{12}\nu_{21}), Q_{12} = \nu_{12}E_2 / (1 - \nu_{12}\nu_{21}), Q_{22} = E_2 / (1 - \nu_{12}\nu_{21}), \quad (2)$$

$$Q_{44} = G_{13}, Q_{55} = G_{23}, Q_{66} = G_{12}$$

where E_1 and E_2 are Young’s moduli in prime material axes; ν_{12} and ν_{21} are Poisson’s ratios.

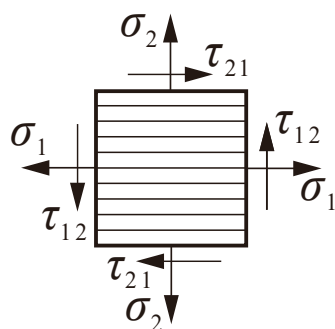


Figure 2. The plane-stress state.

For a unified formulation for each layer, Equation (1) should be transformed into the plate (laminate) coordinate system as

$$\begin{bmatrix} \sigma_x \\ \sigma_y \\ \tau_{xy} \end{bmatrix} = \begin{bmatrix} \bar{Q}_{11} & \bar{Q}_{12} & \bar{Q}_{16} \\ \bar{Q}_{21} & \bar{Q}_{22} & \bar{Q}_{26} \\ \bar{Q}_{61} & \bar{Q}_{62} & \bar{Q}_{66} \end{bmatrix} \begin{bmatrix} \varepsilon_x \\ \varepsilon_y \\ \gamma_{xy} \end{bmatrix}, \begin{bmatrix} \tau_{xz} \\ \tau_{yz} \end{bmatrix} = \begin{bmatrix} \bar{Q}_{44} & \bar{Q}_{45} \\ \bar{Q}_{54} & \bar{Q}_{55} \end{bmatrix} \begin{bmatrix} \gamma_{xz} \\ \gamma_{yz} \end{bmatrix}, \quad (3)$$

in which \bar{Q}_{ij} denotes the modulus component with respect to the plate (laminate) coordinate, and the following relationships are satisfied:

$$\bar{Q}_{12} = \bar{Q}_{21}, \bar{Q}_{16} = \bar{Q}_{61}, \bar{Q}_{26} = \bar{Q}_{62}, \bar{Q}_{45} = \bar{Q}_{54}. \quad (4)$$

2.2. Arrangement of Virtual Boundary Springs

To model the flexural vibration behavior of composite laminates, the first-order shear deformation laminate theory is adopted, and the displacement field is given by

$$\begin{aligned} u_1(x, y, z) &= -z\varphi_x(x, y) \\ u_2(x, y, z) &= -z\varphi_y(x, y) \\ u_3(x, y, z) &= w(x, y) \end{aligned} \quad (5)$$

where $u_1, u_2,$ and u_3 are displacement components with respect to the three global axes $x, y, z,$ respectively; w the deflection of a point on the middle surface. Based on the linear elastic theory, the strain components in terms of displacements can be defined as

$$\begin{aligned} \varepsilon_b &= [\varepsilon_x \ \varepsilon_y \ \gamma_{xy}]^T = -z \left[\frac{\partial \varphi_x}{\partial x} \quad \frac{\partial \varphi_y}{\partial y} \quad \frac{\partial \varphi_x}{\partial y} + \frac{\partial \varphi_y}{\partial x} \right]^T \\ \varepsilon_s &= [\gamma_{xz} \ \gamma_{yz}]^T = \left[\frac{\partial w}{\partial x} - \varphi_x \quad \frac{\partial w}{\partial y} - \varphi_y \right]^T \end{aligned} \quad (6)$$

According to the basic assumptions of the virtual boundary spring technique, all the classical boundary conditions can be imposed by setting extremely large or small stiffnesses to the corresponding boundary springs, and any elastic boundary can be simulated by assigning reasonable and moderate values to the boundary spring stiffness. In FSDT, there are three generalized DOFs, namely, the deflection w and two rotations of the normal line φ_x and φ_y . Therefore, one line spring and two torsion springs linking the laminates with the foundation are arranged on each edge to restrain the three DOFs, as illustrated in Figure 3. The four edges $x = 0, y = 0, x = a,$ and $y = b$ are numbered 1, 2, 3, and 4, respectively. For clarity, Figure 3 only gives a detailed illustration of boundary spring arrangements at sides 2 and 3.

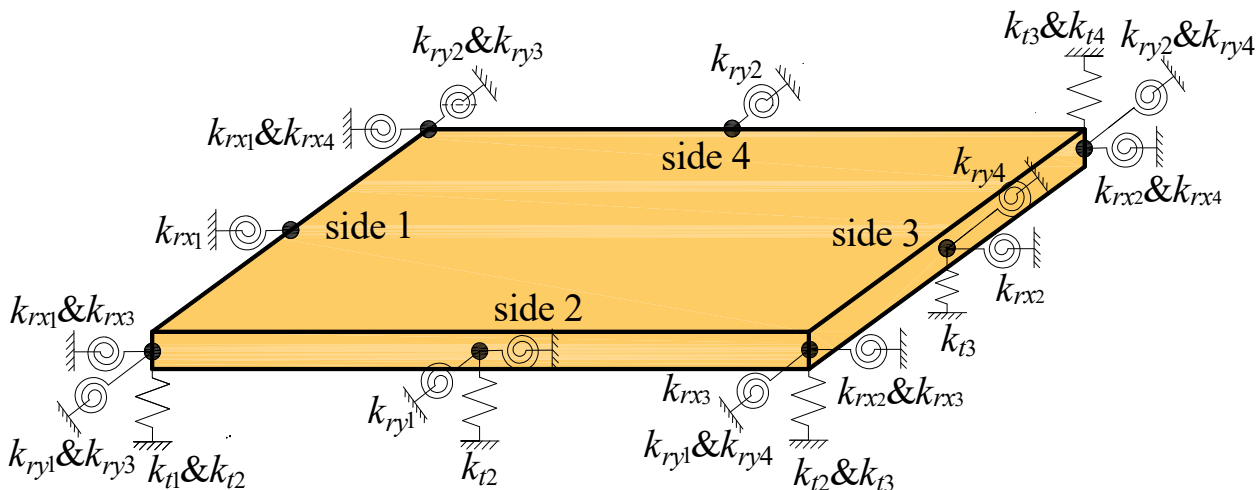


Figure 3. Arrangement of boundary springs.

The notations of all the boundary springs are explained in Table 1. The subscript i of line spring stiffness k_{ti} denotes the number of the side where the line spring is located; the subscripts 1 and 2 of torsion springs k_{rx_i} and k_{ry_i} denote restrictions on normal rotations, while 3 and 4 indicate constraints on tangent rotations.

Table 1. Notations and definitions of boundary springs.

Notations	Definitions
k_{ti} ($i = 1,2,3,4$)	Line spring of the i -th edge
k_{rx_i} ($i = 1,2$)	Torsion springs restricting normal rotations of edges 1 and 3
k_{ry_i} ($i = 1,2$)	Torsion springs restricting normal rotations of edges 2 and 4
k_{rx_i} ($i = 3,4$)	Torsion springs restricting tangent rotations of edges 2 and 4
k_{ry_i} ($i = 3,4$)	Torsion springs restricting tangent rotations of edges 1 and 3

2.3. Rectangular Plate Element

The previous studies [17,18] have shown that the DQFEM can afford highly accurate results even if the entire structure is modeled by very few elements, which is mainly attributed to the use of higher-order polynomials. In addition, the widely used Gauss–Lobatto points have proved to be better than the equally spaced Chebyshev and Legendre points [31–33] in boundary value problems. Therefore, in the present work, the whole plate is divided into just one element, with $M \times N$ Gauss–Lobatto nodes distributed in the domain, as shown in Figure 4.

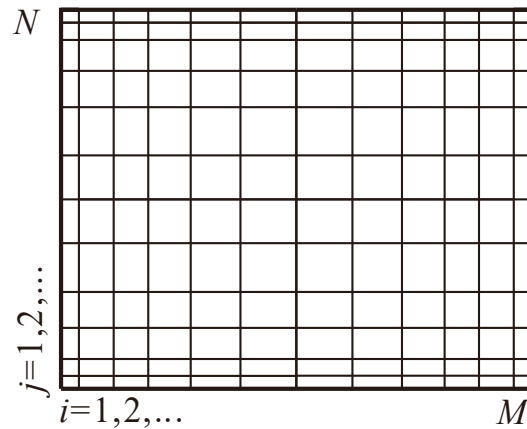


Figure 4. The distributions of grid nodes.

Introducing the Lagrange polynomials as the trial functions, the three generalized displacements can be expressed as

$$\begin{aligned} w(x, y) &= \sum_{i=1}^M \sum_{j=1}^N l_i(x) l_j(y) w_{ij} \\ \varphi_x(x, y) &= \sum_{i=1}^M \sum_{j=1}^N l_i(x) l_j(y) \varphi_{xij} \\ \varphi_y(x, y) &= \sum_{i=1}^M \sum_{j=1}^N l_i(x) l_j(y) \varphi_{yij} \end{aligned} \quad (7)$$

in which l_i and l_j are the Lagrange polynomials, and w_{ij} , φ_{xij} , and φ_{yij} are the deflections and rotations of the Gauss–Lobatto nodes (x_i, y_i) .

To obtain the governing equations, Hamilton's principle is adopted:

$$\delta\Pi = \delta(U + V - T) = 0, \quad (8)$$

where δ is the symbol of variation, and the total potential energy Π consists of the strain energy U , the potential energy of boundary springs V , and the kinetic energy T .

For flexural vibrations of composite laminates, the strain energy can be expressed as the sum of each layer as

$$U = \frac{1}{2} \sum_{i=1}^j \int_{z_i}^{z_{i+1}} \int_A (\boldsymbol{\varepsilon}_b^T \mathbf{D}_b^{(i)} \boldsymbol{\varepsilon}_b + \kappa \boldsymbol{\varepsilon}_s^T \mathbf{D}_s^{(i)} \boldsymbol{\varepsilon}_s) dA dz, \quad (9)$$

in which j is the number of layers; κ is the shear correction factor; z_i and z_{i+1} denote the z coordinates of the top and bottom surfaces of the i -th layer in the Cartesian coordinate system; and $\mathbf{D}_b^{(i)}$ and $\mathbf{D}_s^{(i)}$ represent bending and shear rigidity matrices of the i -th layer in the forms of

$$\mathbf{D}_b^{(i)} = \begin{bmatrix} \bar{Q}^{(i)}_{11} & \bar{Q}^{(i)}_{12} & \bar{Q}^{(i)}_{16} \\ \bar{Q}^{(i)}_{21} & \bar{Q}^{(i)}_{22} & \bar{Q}^{(i)}_{26} \\ \bar{Q}^{(i)}_{61} & \bar{Q}^{(i)}_{62} & \bar{Q}^{(i)}_{66} \end{bmatrix}, \quad \mathbf{D}_s^{(i)} = \begin{bmatrix} \bar{Q}^{(i)}_{44} & \bar{Q}^{(i)}_{45} \\ \bar{Q}^{(i)}_{54} & \bar{Q}^{(i)}_{55} \end{bmatrix}. \quad (10)$$

Considering that the boundary springs are arranged continually on four edges, elastic potential energy stored in the boundary springs can be given in the integral form as

$$V = V_t + V_{rx} + V_{ry} = \frac{1}{2} \sum_{i=1}^4 \int_0^{s_i} (k_{ti} w_i^2 + k_{rxi} \varphi_{xi}^2 + k_{ryi} \varphi_{yi}^2) ds, \quad (11)$$

in which s_i denotes the length of the i -th side; w_i , φ_{xi} , and φ_{yi} represent the deflection and rotations of the i -th side.

Since the displacement field is continuous through the thickness, thus, the kinetic energy of the laminate can be written as

$$T = \frac{1}{2} \iint_A \rho \omega^2 (h w^2 + J \varphi_x^2 + J \varphi_y^2) dx dy, \tag{12}$$

in which ρ is the density of the laminate, and $J = h^3/12$ the axial moment of inertia; ω is the radial frequency of free vibration.

It needs to be pointed out that the potential energy stored in boundary springs is included in the total energy functional, and this special scheme has already taken boundary conditions into account; thus, during the subsequent solution procedures, no additional measures are required to process boundary conditions.

Three generalized node displacement vectors as defined as

$$\begin{aligned} \bar{\varphi}_x^T &= [\varphi_{x11} \ \cdots \ \varphi_{xM1} \ \varphi_{x12} \ \cdots \ \varphi_{xM2} \ \cdots \ \cdots \ \varphi_{x1N} \ \cdots \ \varphi_{xMN}] \\ \bar{\varphi}_y^T &= [\varphi_{y11} \ \cdots \ \varphi_{yM1} \ \varphi_{y12} \ \cdots \ \varphi_{yM2} \ \cdots \ \cdots \ \varphi_{y1N} \ \cdots \ \varphi_{yMN}] \\ \bar{w}^T &= [w_{11} \ \cdots \ w_{M1} \ w_{12} \ \cdots \ w_{M2} \ \cdots \ \cdots \ w_{1N} \ \cdots \ w_{MN}] \end{aligned} \tag{13}$$

Then, using the two-dimensional DQ rule in conjunction with the Gauss–Lobatto integration rule, the strain energy U , the potential energy of boundary springs V , and the kinetic energy T are further expressed in a simpler form as

$$U = \frac{1}{2} \sum_{i=1}^j \frac{z_{i+1}^3 - z_i^3}{3} \left\{ \begin{aligned} &\bar{Q}^{(i)}_{11} \bar{\varphi}_x^T \bar{A}^{(1)T} \bar{C} \bar{A}^{(1)} \bar{\varphi}_x + \bar{Q}^{(i)}_{12} \bar{\varphi}_x^T \bar{A}^{(1)T} \bar{C} \bar{B}^{(1)} \bar{\varphi}_y \\ &+ \bar{Q}^{(i)}_{21} \bar{\varphi}_y^T \bar{B}^{(1)T} \bar{C} \bar{A}^{(1)} \bar{\varphi}_x + \bar{Q}^{(i)}_{22} \bar{\varphi}_y^T \bar{B}^{(1)T} \bar{C} \bar{B}^{(1)} \bar{\varphi}_y \\ &+ \bar{Q}^{(i)}_{16} \bar{\varphi}_x^T \bar{A}^{(1)T} \bar{C} (\bar{B}^{(1)} \bar{\varphi}_x + \bar{A}^{(1)} \bar{\varphi}_y) \\ &+ \bar{Q}^{(i)}_{26} \bar{\varphi}_y^T \bar{B}^{(1)T} \bar{C} (\bar{B}^{(1)} \bar{\varphi}_x + \bar{A}^{(1)} \bar{\varphi}_y) \\ &+ \bar{Q}^{(i)}_{61} (\bar{\varphi}_x^T \bar{B}^{(1)T} \bar{C} + \bar{\varphi}_y^T \bar{A}^{(1)T} \bar{C}) \bar{A}^{(1)} \bar{\varphi}_x \\ &+ \bar{Q}^{(i)}_{62} (\bar{\varphi}_x^T \bar{B}^{(1)T} \bar{C} + \bar{\varphi}_y^T \bar{A}^{(1)T} \bar{C}) \bar{B}^{(1)} \bar{\varphi}_y \\ &+ \bar{Q}^{(i)}_{66} (\bar{\varphi}_x^T \bar{B}^{(1)T} + \bar{\varphi}_y^T \bar{A}^{(1)T}) \bar{C} (\bar{B}^{(1)} \bar{\varphi}_x + \bar{A}^{(1)} \bar{\varphi}_y) \end{aligned} \right\}, \tag{14}$$

$$+ \frac{1}{2} \sum_{i=1}^j \frac{z_{i+1} - z_i}{3} \kappa \left\{ \begin{aligned} &\bar{Q}^{(i)}_{44} (\bar{w}^T \bar{A}^{(1)T} - \bar{\varphi}_x^T) \bar{C} (\bar{A}^{(1)} \bar{w} - \bar{\varphi}_x) \\ &+ \bar{Q}^{(i)}_{45} (\bar{w}^T \bar{A}^{(1)T} - \bar{\varphi}_x^T) \bar{C} (\bar{B}^{(1)} \bar{w} - \bar{\varphi}_y) \\ &+ \bar{Q}^{(i)}_{54} (\bar{w}^T \bar{B}^{(1)T} - \bar{\varphi}_y^T) \bar{C} (\bar{A}^{(1)} \bar{w} - \bar{\varphi}_x) \\ &+ \bar{Q}^{(i)}_{55} (\bar{w}^T \bar{B}^{(1)T} - \bar{\varphi}_y^T) \bar{C} (\bar{B}^{(1)} \bar{w} - \bar{\varphi}_y) \end{aligned} \right\}$$

$$V = \frac{1}{2} \left(\sum_{i=1}^4 \bar{w}^T \bar{C} \bar{K}_{ii} \bar{w} + \sum_{i=1}^4 \bar{\varphi}_x^T \bar{C} \bar{K}_{rxi} \bar{\varphi}_x + \sum_{i=1}^4 \bar{\varphi}_y^T \bar{C} \bar{K}_{ryi} \bar{\varphi}_y \right), \tag{15}$$

$$T = \frac{1}{2} \rho \omega^2 (h \bar{w}^T \bar{C} \bar{w} + J \bar{\varphi}_x^T \bar{C} \bar{\varphi}_x + J \bar{\varphi}_y^T \bar{C} \bar{\varphi}_y), \tag{16}$$

in which $\bar{A}^{(1)}$ and $\bar{B}^{(1)}$ are weighting coefficient matrices given in Appendix A, and the matrices \bar{C} , \bar{K}_{ii} , \bar{K}_{rxi} , and \bar{K}_{ryi} ($i = 1, 2, 3, 4$) are defined as follows

$$\bar{C} = \text{diag} [C_1^x C_1^y, \dots, C_M^x C_1^y, C_1^x C_2^y, \dots, C_M^x C_2^y, \dots, C_1^x C_N^y, \dots, C_M^x C_N^y], \tag{17}$$

$$\begin{aligned}
 \bar{K}_{t1} &= \text{diag}(\overbrace{K_{t1}, K_{t1}, \dots, K_{t1}}^N), K_{t1} = \text{diag}(\overbrace{k_{t1}, 0, \dots, 0}^{M-1}) \\
 \bar{K}_{t2} &= \text{diag}(\overbrace{k_{t2}, k_{t2}, \dots, k_{t2}}^N, \overbrace{0, \dots, 0}^{(N-1)M}), \\
 \bar{K}_{t3} &= \text{diag}(\overbrace{K_{t3}, K_{t3}, \dots, K_{t3}}^{(N-1)M}, \overbrace{K_{t3}}^M, K_{t3} = \text{diag}(\overbrace{0, \dots, 0, k_{t3}}^{M-1}), \\
 \bar{K}_{t4} &= \text{diag}(\overbrace{0, \dots, 0}^{(N-1)M}, \overbrace{k_{t4}, k_{t4}, \dots, k_{t4}}^M)
 \end{aligned} \tag{18}$$

$$\begin{aligned}
 \bar{K}_{rx1} &= \text{diag}(\overbrace{K_{rx1}, K_{rx1}, \dots, K_{rx1}}^N), K_{rx1} = \text{diag}(\overbrace{k_{rx1}, 0, \dots, 0}^{M-1}) \\
 \bar{K}_{rx2} &= \text{diag}(\overbrace{K_{rx2}, K_{rx2}, \dots, K_{rx2}}^N), K_{rx2} = \text{diag}(\overbrace{0, \dots, 0, k_{rx2}}^{M-1}), \\
 \bar{K}_{ry1} &= \text{diag}(\overbrace{k_{ry1}, k_{ry1}, \dots, k_{ry1}}^{(N-1)M}, \overbrace{0, \dots, 0}^M) \\
 \bar{K}_{ry2} &= \text{diag}(\overbrace{0, \dots, 0}^{(N-1)M}, \overbrace{k_{ry2}, k_{ry2}, \dots, k_{ry2}}^M)
 \end{aligned} \tag{19}$$

$$\begin{aligned}
 \bar{K}_{ry3} &= \text{diag}(\overbrace{K_{ry3}, K_{ry3}, \dots, K_{ry3}}^N), K_{ry3} = \text{diag}(\overbrace{k_{ry3}, 0, \dots, 0}^{M-1}) \\
 \bar{K}_{ry4} &= \text{diag}(\overbrace{K_{ry4}, K_{ry4}, \dots, K_{ry4}}^N), K_{ry4} = \text{diag}(\overbrace{0, \dots, 0, k_{ry4}}^{M-1}), \\
 \bar{K}_{rx3} &= \text{diag}(\overbrace{k_{rx3}, k_{rx3}, \dots, k_{rx3}}^{(N-1)M}, \overbrace{0, \dots, 0}^M) \\
 \bar{K}_{rx4} &= \text{diag}(\overbrace{0, \dots, 0}^{(N-1)M}, \overbrace{k_{rx4}, k_{rx4}, \dots, k_{rx4}}^M)
 \end{aligned} \tag{20}$$

where C_M^x and C_N^y given in Equation (A6) are the M -th and N -th Gauss–Lobatto weights with respect to x and y , respectively.

Define a displacement vector as

$$w = [\bar{\varphi}_x^T \quad \bar{\varphi}_y^T \quad \bar{w}^T]^T \tag{21}$$

Then the total potential energy can be further written in a compact form as

$$\Pi = \frac{1}{2} w^T K w - \frac{1}{2} \omega^2 w^T M w, \tag{22}$$

where the stiffness matrix K and mass matrix M are given by

$$K = K_U + K_V, M = \rho \text{diag}(JC, JC, hC), \tag{23}$$

in which K_U and K_V account for the contributions of the strain energy and elastic potential energy of boundary springs, respectively, which are obtained as

$$K_U = \begin{bmatrix} K_{11} & K_{12} & K_{13} \\ K_{21} & K_{22} & K_{23} \\ K_{31} & K_{32} & K_{33} \end{bmatrix}, K_V = \text{diag}(\sum_{i=1}^4 C \bar{K}_{rxi}, \sum_{i=1}^4 C \bar{K}_{ryi}, \sum_{i=1}^4 C \bar{K}_{ti}). \tag{24}$$

The matrices in expressions of K_U are given below.

$$\begin{aligned}
 \mathbf{K}_{11} &= \frac{1}{2} \sum_{i=1}^j \frac{z_{i+1}^3 - z_i^3}{3} \left(\bar{Q}^{(i)}_{11} \bar{\mathbf{A}}^{(1)\text{T}} \mathbf{C} \bar{\mathbf{A}}^{(1)} + \bar{Q}^{(i)}_{16} \bar{\mathbf{A}}^{(1)\text{T}} \mathbf{C} \bar{\mathbf{B}}^{(1)} \right. \\
 &\quad \left. + \bar{Q}^{(i)}_{61} \bar{\mathbf{B}}^{(1)\text{T}} \mathbf{C} \bar{\mathbf{A}}^{(1)} + \bar{Q}^{(i)}_{66} \bar{\mathbf{B}}^{(1)\text{T}} \mathbf{C} \bar{\mathbf{B}}^{(1)} \right) + \frac{1}{2} \sum_{i=1}^j \frac{z_{i+1} - z_i}{3} \kappa \bar{Q}^{(i)}_{44} \mathbf{C} \\
 \mathbf{K}_{12} &= \frac{1}{2} \sum_{i=1}^j \frac{z_{i+1}^3 - z_i^3}{3} \left\{ \begin{aligned} &(\bar{Q}^{(i)}_{12} + \bar{Q}^{(i)}_{21} + \bar{Q}^{(i)}_{66}) \bar{\mathbf{A}}^{(1)\text{T}} \mathbf{C} \bar{\mathbf{B}}^{(1)} \\ &+ (\bar{Q}^{(i)}_{61} + \bar{Q}^{(i)}_{16}) \bar{\mathbf{A}}^{(1)\text{T}} \mathbf{C} \bar{\mathbf{A}}^{(1)} \\ &+ (\bar{Q}^{(i)}_{26} + \bar{Q}^{(i)}_{62}) \bar{\mathbf{B}}^{(1)\text{T}} \mathbf{C} \bar{\mathbf{B}}^{(1)} \\ &+ \bar{Q}^{(i)}_{66} \bar{\mathbf{B}}^{(1)\text{T}} \mathbf{C} \bar{\mathbf{A}}^{(1)} \end{aligned} \right\} + \frac{1}{2} \sum_{i=1}^j \frac{z_{i+1} - z_i}{3} \kappa \bar{Q}^{(i)}_{54} \mathbf{C} \\
 \mathbf{K}_{13} &= -\frac{1}{2} \sum_{i=1}^j \frac{z_{i+1} - z_i}{3} \kappa (\bar{Q}^{(i)}_{44} \mathbf{C} \bar{\mathbf{A}}^{(1)} + \bar{Q}^{(i)}_{45} \mathbf{C} \bar{\mathbf{B}}^{(1)}) \\
 \mathbf{K}_{21} &= \frac{1}{2} \sum_{i=1}^j \frac{z_{i+1}^3 - z_i^3}{3} \left\{ \begin{aligned} &(\bar{Q}^{(i)}_{12} + \bar{Q}^{(i)}_{21} + \bar{Q}^{(i)}_{66}) \bar{\mathbf{B}}^{(1)\text{T}} \mathbf{C} \bar{\mathbf{A}}^{(1)} \\ &+ (\bar{Q}^{(i)}_{61} + \bar{Q}^{(i)}_{16}) \bar{\mathbf{A}}^{(1)\text{T}} \mathbf{C} \bar{\mathbf{A}}^{(1)} \\ &+ (\bar{Q}^{(i)}_{26} + \bar{Q}^{(i)}_{62}) \bar{\mathbf{B}}^{(1)\text{T}} \mathbf{C} \bar{\mathbf{B}}^{(1)} \\ &+ \bar{Q}^{(i)}_{66} \bar{\mathbf{A}}^{(1)\text{T}} \mathbf{C} \bar{\mathbf{B}}^{(1)} \end{aligned} \right\} + \frac{1}{2} \sum_{i=1}^j \frac{z_{i+1} - z_i}{3} \kappa \bar{Q}^{(i)}_{54} \mathbf{C} \\
 \mathbf{K}_{22} &= \frac{1}{2} \sum_{i=1}^j \frac{z_{i+1}^3 - z_i^3}{3} \left\{ \begin{aligned} &\bar{Q}^{(i)}_{22} \bar{\mathbf{B}}^{(1)\text{T}} \mathbf{C} \bar{\mathbf{B}}^{(1)} + \bar{Q}^{(i)}_{26} \bar{\mathbf{B}}^{(1)\text{T}} \mathbf{C} \bar{\mathbf{A}}^{(1)} \\ &+ \bar{Q}^{(i)}_{62} \bar{\mathbf{A}}^{(1)\text{T}} \mathbf{C} \bar{\mathbf{B}}^{(1)} + \bar{Q}^{(i)}_{66} \bar{\mathbf{A}}^{(1)\text{T}} \mathbf{C} \bar{\mathbf{A}}^{(1)} \end{aligned} \right\} + \frac{1}{2} \sum_{i=1}^j \frac{z_{i+1} - z_i}{3} \kappa \bar{Q}^{(i)}_{55} \mathbf{C} \\
 \mathbf{K}_{23} &= -\frac{1}{2} \sum_{i=1}^j \frac{z_{i+1} - z_i}{3} \kappa (\bar{Q}^{(i)}_{54} \mathbf{C} \bar{\mathbf{A}}^{(1)} + \bar{Q}^{(i)}_{55} \mathbf{C} \bar{\mathbf{B}}^{(1)}) \\
 \mathbf{K}_{31} &= -\frac{1}{2} \sum_{i=1}^j \frac{z_{i+1} - z_i}{3} \kappa (\bar{Q}^{(i)}_{44} \bar{\mathbf{A}}^{(1)\text{T}} \mathbf{C} + \bar{Q}^{(i)}_{54} \bar{\mathbf{B}}^{(1)\text{T}} \mathbf{C}) \\
 \mathbf{K}_{32} &= -\frac{1}{2} \sum_{i=1}^j \frac{z_{i+1} - z_i}{3} \kappa (\bar{Q}^{(i)}_{54} \bar{\mathbf{A}}^{(1)\text{T}} \mathbf{C} + \bar{Q}^{(i)}_{55} \bar{\mathbf{B}}^{(1)\text{T}} \mathbf{C}) \\
 \mathbf{K}_{33} &= \frac{1}{2} \sum_{i=1}^j \frac{z_{i+1} - z_i}{3} \kappa \left(\bar{Q}^{(i)}_{44} \bar{\mathbf{A}}^{(1)\text{T}} \mathbf{C} \bar{\mathbf{A}}^{(1)} + \bar{Q}^{(i)}_{45} \bar{\mathbf{A}}^{(1)\text{T}} \mathbf{C} \bar{\mathbf{B}}^{(1)} \right. \\
 &\quad \left. + \bar{Q}^{(i)}_{54} \bar{\mathbf{B}}^{(1)\text{T}} \mathbf{C} \bar{\mathbf{A}}^{(1)} + \bar{Q}^{(i)}_{55} \bar{\mathbf{B}}^{(1)\text{T}} \mathbf{C} \bar{\mathbf{B}}^{(1)} \right)
 \end{aligned} \tag{25}$$

The DQFEM formulation for free vibration analysis of composite laminate is eventually equivalent to an eigenvalue problem governed by a standard characteristic equation obtained from the Hamilton’s principle as

$$(\mathbf{K} - \omega^2 \mathbf{M}) \mathbf{w} = 0 \tag{26}$$

It is noteworthy that the stiffness matrix \mathbf{K} and mass matrix \mathbf{M} are nonsingular due to the inclusion of boundary spring potential energy into the energy functional; thus, the characteristic Equation as (26) can be directly solved without reducing the order of the matrix in this equation, and the directly obtained modal vector is complete. Moreover, the boundary conditions can be conveniently changed simply by altering the boundary spring stiffness, without the need of researching and eliminating the zero DOFs.

3. Numerical Examples and Discussions

To investigate the convergence characteristics and accuracy of the modified DQFEM in application to flexural vibrations of composite laminates, a series of numerical examples are carried out.

In the following numerical examples, the shear correction factor κ is taken as $\pi^2/12$, and a three-layered symmetric cross-ply laminate with the stacking sequence $0^\circ/90^\circ/0^\circ$ is considered. The elastic constants of each single-layer are given as [34,35]

$$E_1/E_2 = \nu_{12}/\nu_{21} = 40, G_{12} = G_{13} = 0.6E_2, G_{23} = 0.5E_2, \nu_{12} = 0.25$$

To facilitate comparison with other published results, a nondimensional natural frequency parameter is defined as [34,35]

$$\Omega = (\omega b^2 / \pi^2) \sqrt{\rho h / D_0}, \tag{27}$$

in which $D_0 = E_2 h^3 / 12(1 - \nu_{12} \nu_{21})$.

3.1. Convergence Characteristics

To obtain the required number of Gauss–Lobatto nodes to ensure convergent results and the recommended values of virtual boundary spring stiffnesses that make the boundaries strictly constrained, the convergence characteristics of the present method are investigated, covering both thin ($h/b = 0.001$) and thick ($h/b = 0.2$) geometries. Additionally, the specific cases of two boundary combinations, i.e., CCCC and SSSS, are considered. For these two cases, the virtual spring stiffnesses of all the four boundaries are identical. Note that for the sake of clarity, the line spring stiffness is denoted by k_t , and the stiffnesses of torsion springs that restrict the normal rotation and tangent rotation are referred to as k_{r1} and k_{r2} , respectively.

3.1.1. Varying the Number of Gauss–Lobatto Nodes

In order to facilitate the calculation, set the same number of Gauss–Lobatto nodes along the x - and y -direction. To simulate CCCC boundary combinations, theoretically, the stiffnesses of all line and torsion springs should be assigned infinitely large values to restrict both translational and rotational DOFs of all boundaries. However, infinite values cannot be processed by numerical computations; thus, a relatively large value (i.e., 10^8) is assigned instead. Similarly, to model SSSS laminates, the stiffnesses of all line springs k_t and tangent torsion springs k_{r2} should be infinitely large to restrict the transverse deflections and tangent rotations of all edges, and a large value of 10^8 is assigned to them, while the stiffness of normal torsion springs k_{r1} should be zero to set the normal rotation free.

For square laminates ($h/b = 0.001$ and 0.2) with CCCC and SSSS boundary combinations, the variations of nondimensional natural frequencies versus the number of unilateral Gauss–Lobatto nodes are depicted in Figures 5 and 6, in which the fiducial lines indicate the convergence values of frequency parameters. Note that in the present paper, if the result with three decimal digits reaches a constant value, the calculation is seen as converged. One can find from Figures 5 and 6 that for both CCCC and SSSS plates, the minimum number of unilateral nodes required to make the nondimensional frequencies converge is 11 when $h/b = 0.001$ and 0.2 .

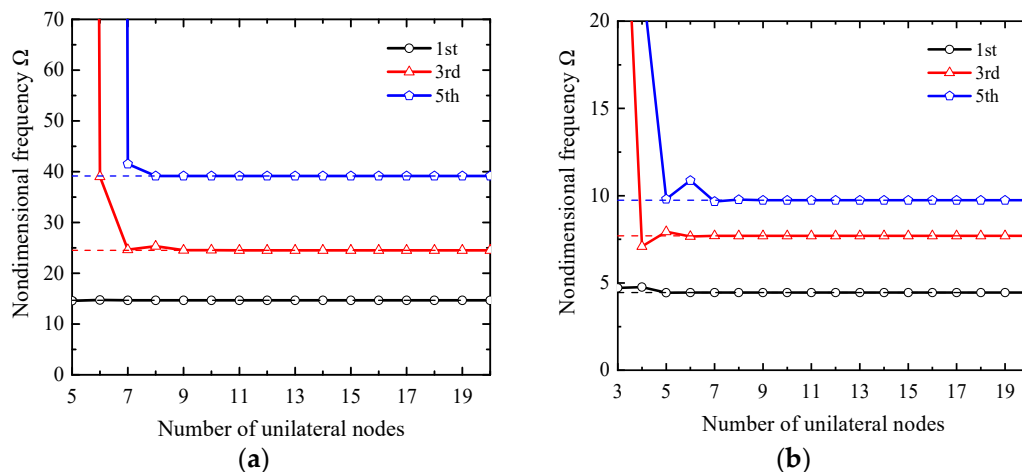


Figure 5. Variations of nondimensional frequencies Ω for CCCC laminates ($0^\circ, 90^\circ, 0^\circ$) versus the number of nodes: (a) $h/b = 0.001, k_t = k_{r1} = k_{r2} = 10^8$; (b) $h/b = 0.2, k_t = k_{r1} = k_{r2} = 10^8$.

To sum up, the modified DQFEM is capable of yielding convergent results with only a few Gauss–Lobatto nodes required. In the following calculation for square laminates with thickness ratios between 0.001 and 0.2, the number of nodes per side is taken as 11 to ensure good convergence without sacrificing computational efficiency.

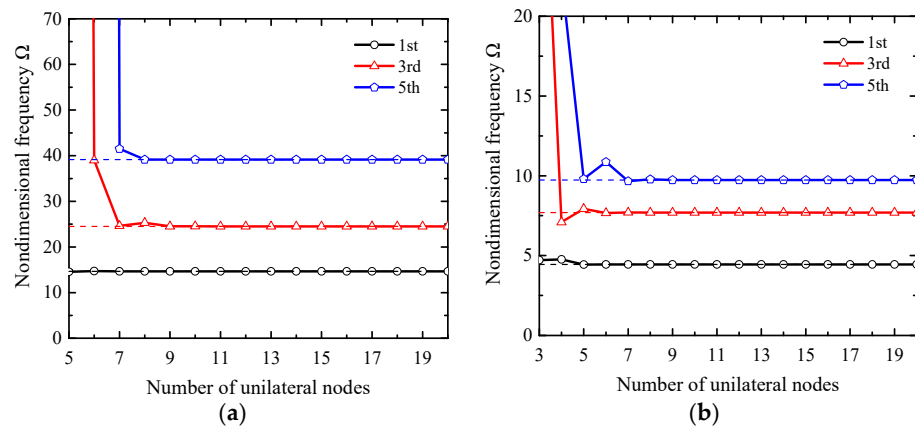


Figure 6. Variations of nondimensional frequencies Ω for SSSS laminates ($0^\circ, 90^\circ, 0^\circ$) versus the number of nodes: (a) $h/b = 0.001, k_t = k_{r2} = 10^8, k_{r1} = 0$; (b) $h/b = 0.2, k_t = k_{r2} = 10^8, k_{r1} = 0$.

3.1.2. Effect of the Boundary Spring Stiffness on Convergence

For the convenience of calculation, we assign the same value k to the stiffnesses of boundary springs corresponding to the DOFs that need to be strictly constrained. For instance, set $k_t = k_{r1} = k_{r2} = k$, when simulating a clamped edge, and $k_t = k_{r2} = k, k_{r1} = 0$ for a simply supported edge. During the calculation, set $M = N = 11$.

Figures 7 and 8 display the variations of nondimensional frequencies with respect to k when simulating boundary combinations of CCCC and SSSS. The straight line with an arrow points to the lower limit of k that makes the first five frequency parameters with four significant digits converge.

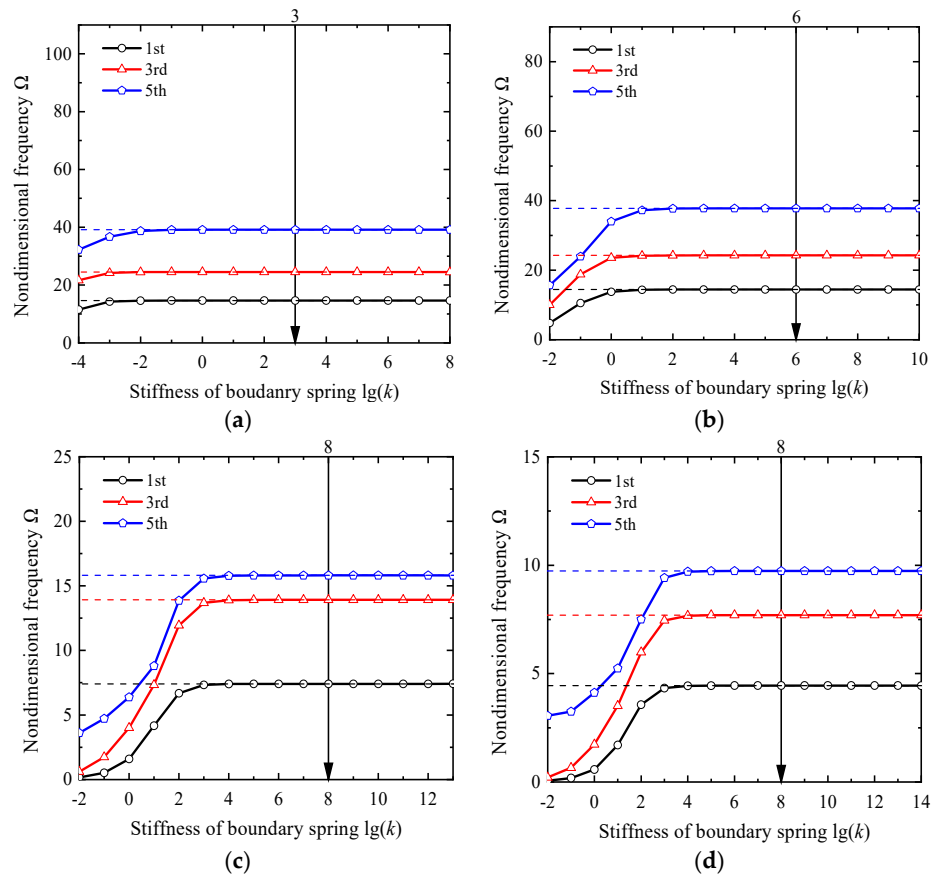


Figure 7. Variations of nondimensional frequencies Ω for CCCC laminates ($0^\circ, 90^\circ, 0^\circ$) versus the stiffness of boundary spring ($k_t = k_{r1} = k_{r2} = k$): (a) $h/b = 0.001$; (b) $h/b = 0.01$; (c) $h/b = 0.1$; (d) $h/b = 0.2$.

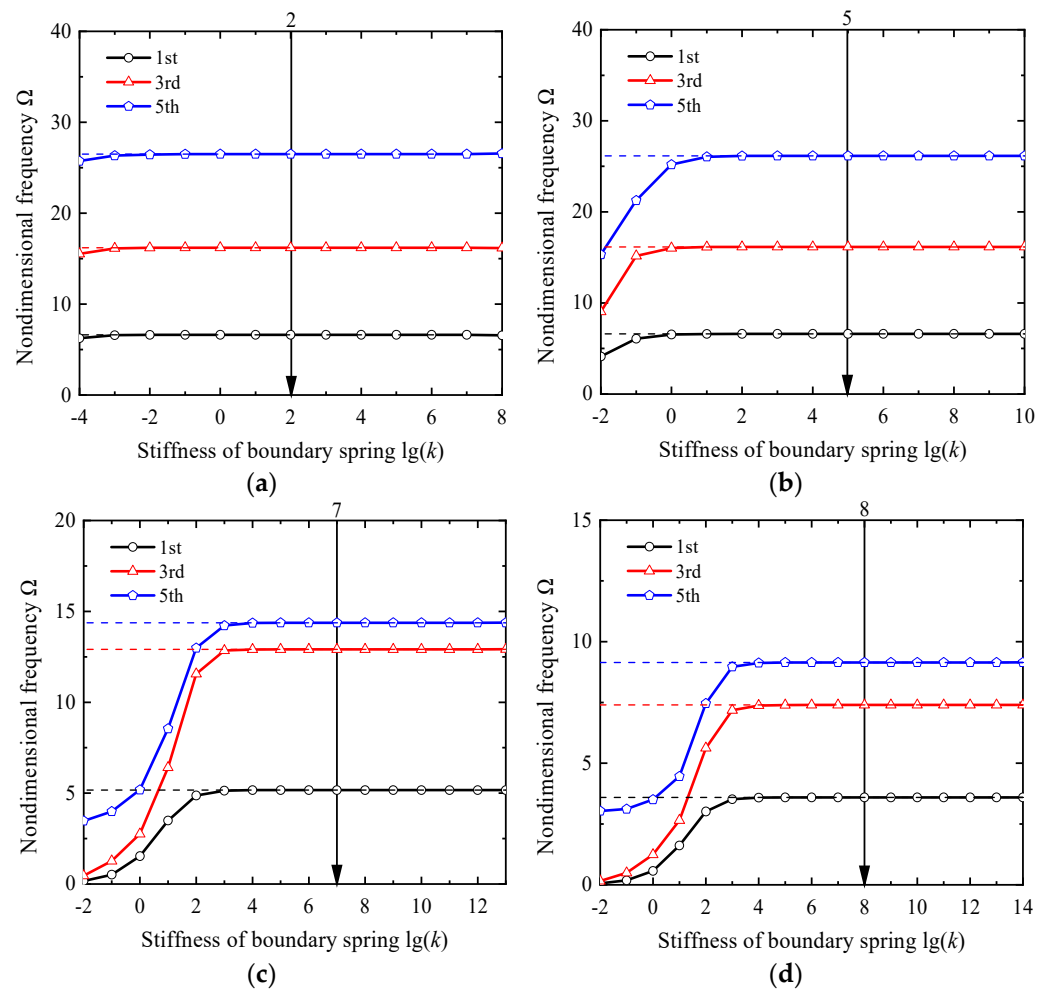


Figure 8. Variations of nondimensional frequencies Ω for SSSS laminates ($0^\circ, 90^\circ, 0^\circ$) versus the stiffness of boundary spring ($k_t = k_{r2} = k, k_{r1} = 0$): (a) $h/b = 0.001$; (b) $h/b = 0.01$; (c) $h/b = 0.1$; (d) $h/b = 0.2$.

As is seen in Figures 7 and 8, for both CCCC and SSSS laminates with various thickness ratios ranging from 0.001 to 0.2, the frequencies experience an increase when k is relatively small so as to simulate the general elastic restraints, and the increase rate grows as the plate gets thicker. When k reaches a certain value (for instance $k = 10^2$ when $h/b = 0.01$), the frequencies will remain almost constant; this observation coincides with the basic assumption that when the spring stiffness is large enough, the corresponding DOF can be considered as strictly restricted so as to simulate the classical boundary conditions. It is noteworthy that for composite laminates with a thin geometry ($h/b = 0.001$ and 0.01), the frequency parameters are slightly influenced by the value of k as long as it is larger than 10, while the frequencies of moderately thick laminates ($h/b = 0.1$ and 0.2) are more susceptible to k .

Table 2 lists the optimal values of the boundary spring stiffnesses for clamped and simply supported boundaries. It should be emphasized that the lower limit of k is rigorously determined by the point where the first five frequency parameters accurately converge to four decimal places. This may not be clearly shown in Figures 7 and 8 due to the slight variation in the nondimensional frequency during the stationary part of the curve.

One can also see that the spring stiffness in Table 2 varies from 10^3 to 10^8 , which is totally within the calculation ability of a personal computer. Additionally, there is an associated increase in the recommended value of k as the plate thickness increases. It should be pointed out the calculation may not converge if k is below the recommended value, and numerically ill-conditioned problems may occur if k is too large.

Table 2. Optimal values of the stiffness k for boundary springs of laminates (0° , 90° , 0°).

Thickness Ratio h/b	CCCC	SSSS
0.001	10^3	10^2
0.01	10^6	10^5
0.1	10^8	10^7
0.2	10^8	10^8

3.2. Composite Laminates with Classical Boundary Conditions

3.2.1. Verification of Accuracy

To demonstrate the accuracy of Ω estimated from the modified DQFEM, a series of numerical comparisons is performed.

As is known, more accurate solutions can be generated by increasing Gauss–Lobatto nodes, but higher requirements on computing resources will be caused at the same time. Therefore, taking both accuracy and computational cost into account, and according to the discussions of the convergence characteristics above, 11×11 Gauss–Lobatto nodes are selected to discretize the square laminates in the following numerical examples. The values of boundary spring stiffnesses to simulate clamped and simply supported boundaries corresponding to various thickness ratios are listed in Table 3.

Table 3. Boundary spring stiffness for clamped and simply supported boundary.

Thickness Ratio h/b	The Stiffness k of Boundary Spring	
	Clamped Boundary (C)	Simply Supported Boundary (S)
0.001	10^3	10^2
0.01	10^6	10^5
0.05 ¹	10^7	10^6
0.1	10^8	10^7
0.15 ¹	10^8	$10^{7.5}$
0.2	10^8	10^8

¹ The corresponding stiffness are obtained by interpolation.

The first eight nondimensional natural frequencies of square laminates with various thickness ratios are calculated and listed in Tables 4–10, as well as the exact solutions by Liu [34] and numerical solutions generated by the p -Ritz method [35]. Several boundary combinations such as CCCC, SSSS, SCSC, SFSE, SSSF, SSSC, and SCSF are covered. Extensive comparisons show that the present results are highly consistent with the exact solutions for three digits. For most results, the relative errors approach zero. The non-zero relative errors exist in only a very small number of results mostly involving SFSE plates, and the maximum percentage error is less than 0.02% for the worst case. Therefore, the accuracy of the present method in free vibration of composite laminates is verified.

Table 4. The nondimensional frequency Ω for CCCC laminates.

Thickness Ratio h/b	Method	Order of Frequency							
		1st	2nd	3rd	4th	5th	6th	7th	8th
0.001	Present	14.666	17.614	24.511	35.532	39.157	40.768	44.786	50.323
	p -Ritz	14.666	17.614	24.511	35.532	39.157	40.768	44.786	50.297
0.05	Present	10.953	14.028	20.388	23.196	24.978	29.237	29.369	36.266
	p -Ritz	10.953	14.028	20.388	23.196	24.978	29.237	29.369	36.266
0.1	Present	7.411	10.393	13.913	15.429	15.806	19.572	21.489	21.620
	p -Ritz	7.411	10.393	13.913	15.429	15.806	19.572	21.489	21.620
0.15	Present	5.548	8.147	9.904	11.622	12.025	14.645	14.911	16.123
	p -Ritz	5.548	8.147	9.904	11.622	12.025	14.645	14.911	16.123
0.2	Present	4.447	6.642	7.700	9.185	9.738	11.399	11.644	12.466
	p -Ritz	4.447	6.642	7.700	9.185	9.738	11.399	11.644	12.466

Table 5. The nondimensional frequency Ω for SSSS laminates.

Thickness Ratio h/b	Method	Order of Frequency							
		1st	2nd	3rd	4th	5th	6th	7th	8th
0.001	Present	6.625	9.447	16.205	25.115	26.498	26.657	30.314	37.785
	Exact	6.625	9.447	16.205	25.115	26.498	26.657	30.314	37.785
	p -Ritz	6.625	9.447	16.205	25.115	26.498	26.657	30.314	37.785
0.05	Present	6.138	8.888	15.110	19.354	20.665	24.070	24.344	31.028
	Exact	6.138	8.888	15.110	19.354	20.665	24.070	24.344	31.028
	p -Ritz	6.138	8.888	15.110	19.354	20.665	24.070	24.344	31.028
0.1	Present	5.166	7.757	12.915	13.049	14.376	17.788	19.502	21.051
	Exact	5.166	7.757	12.915	13.049	14.376	17.788	19.502	21.051
	p -Ritz	5.166	7.757	12.915	13.049	14.376	17.788	19.502	21.051
0.15	Present	4.275	6.667	9.488	10.824	10.826	13.804	14.665	15.590
	Exact	4.275	6.667	9.488	10.824	10.826	13.804	14.665	15.590
	p -Ritz	4.275	6.667	9.488	10.824	10.826	13.804	14.665	15.590
0.2	Present	3.594	5.769	7.397	8.688	9.145	11.208	11.223	12.117
	Exact	3.594	5.769	7.397	8.688	9.145	11.208	11.223	12.117
	p -Ritz	3.594	5.769	7.397	8.688	9.145	11.208	11.223	12.117

Table 6. The nondimensional frequency Ω for SCSC laminates.

Thickness Ratio h/b	Method	Order of Frequency							
		1st	2nd	3rd	4th	5th	6th	7th	8th
0.05	Present	6.890	11.246	18.664	19.619	21.801	26.689	28.260	34.348
	Exact	6.890	11.246	18.664	19.619	21.801	26.689	28.260	34.348
	p -Ritz	6.890	11.246	18.664	19.619	21.801	26.689	28.260	34.348
0.1	Present	5.871	9.454	13.340	14.878	15.340	19.229	21.231	21.275
	Exact	5.871	9.454	13.340	14.878	15.340	19.229	21.231	21.275
	p -Ritz	5.871	9.454	13.340	14.878	15.340	19.229	21.231	21.275
0.15	Present	4.275	6.667	9.488	10.824	10.826	13.804	14.665	15.590
	Exact	4.275	6.667	9.488	10.824	10.826	13.804	14.665	15.590
	p -Ritz	4.275	6.667	9.488	10.824	10.826	13.804	14.665	15.590
0.2	Present	4.137	6.474	7.664	9.159	9.643	11.377	11.625	12.448
	Exact	4.137	6.474	7.664	9.159	9.643	11.377	11.625	12.448
	p -Ritz	4.137	6.474	7.664	9.159	9.643	11.377	11.625	12.448

Table 7. The nondimensional frequency Ω for SFSF laminates.

Thickness ratio h/b	Method	Order of Frequency							
		1st	2nd	3rd	4th	5th	6th	7th	8th
0.05	Present	5.734	5.933	7.398	11.918	19.124	19.284	19.603	20.087
	Exact	5.734	5.933	7.397	11.917	19.124	19.284	19.602	20.086
	p -Ritz	5.734	5.933	7.397	11.918	19.124	19.284	19.602	20.086
0.1	Present	4.781	4.935	6.320	10.345	12.851	12.959	13.677	16.070
	Exact	4.781	4.935	6.319	10.345	12.851	12.959	13.677	16.070
	p -Ritz	4.781	4.935	6.319	10.345	12.851	12.959	13.677	16.070
0.2	Present	3.213	3.311	4.619	7.195	7.273	7.599	8.004	10.043
	Exact	3.213	3.311	4.619	7.195	7.272	7.599	8.004	10.043
	p -Ritz	3.213	3.311	4.619	7.195	7.272	7.599	8.004	10.043

Although the above convergence study concentrates on CCCC and SSSS plates, one can see from the numerical comparisons that the conclusions regarding the required node number and recommended boundary spring stiffnesses have been successfully extended into the analysis of other boundary conditions. Additionally, it implies that a slight variation in the values of boundary spring stiffnesses within a specific interval might have an influence on the obtained results, but only to a limited extent. Therefore, it can be reasonably

inferred that the present approach is numerically stable and highly accurate, regardless of boundary conditions.

Table 8. The nondimensional frequency Ω for SSSF laminates.

Thickness Ratio h/b	Method	Order of Frequency							
		1st	2nd	3rd	4th	5th	6th	7th	8th
0.05	Present	5.785	6.657	10.301	17.279	19.165	19.655	21.520	25.971
	Exact	5.785	6.657	10.301	17.279	19.165	19.655	21.519	25.970
0.1	Present	4.821	5.641	8.976	12.879	13.304	14.614	15.144	19.121
	Exact	4.821	5.641	8.976	12.879	13.304	14.614	15.144	19.121
0.2	Present	3.240	4.017	6.654	7.216	7.642	9.323	10.195	11.077
	Exact	3.240	4.017	6.654	7.216	7.642	9.323	10.195	11.077

Table 9. The nondimensional frequency Ω for SSSC laminates.

Thickness Ratio h/b	Method	Order of Frequency							
		1st	2nd	3rd	4th	5th	6th	7th	8th
0.05	Present	6.429	9.983	16.848	19.459	21.172	25.460	26.159	32.661
	Exact	6.429	9.983	16.847	19.459	21.172	25.460	26.159	32.661
0.1	Present	5.450	8.587	13.165	13.914	14.832	18.510	20.413	21.123
	Exact	5.450	8.587	13.165	13.914	14.832	18.510	20.412	21.123
0.2	Present	3.835	6.140	7.513	8.931	9.401	11.282	11.429	12.286
	Exact	3.835	6.140	7.513	8.931	9.401	11.282	11.429	12.286

Table 10. The nondimensional frequency Ω for SCSF laminates.

Thickness Ratio h/b	Method	Order of Frequency							
		1st	2nd	3rd	4th	5th	6th	7th	8th
0.05	Present	5.8293	7.1375	11.5836	19.1261	19.1837	19.8523	22.1823	27.2341
	Exact	5.8293	7.1375	11.5836	19.1261	19.1837	19.8523	22.1823	27.2341
0.1	Present	4.8650	6.0724	9.8872	12.8983	13.4994	15.6061	15.6911	19.8715
	Exact	4.8650	6.0724	9.8872	12.8983	13.4994	15.6061	15.6911	19.8715
0.2	Present	3.2877	4.3135	7.0132	7.2389	7.7982	9.5741	10.4079	11.0930
	Exact	3.2877	4.3135	7.0132	7.2389	7.7982	9.5741	10.4079	11.0930

Figure 9 presents the first three modes for SSSS, SCSC, and SSSF laminates with $h/b = 0.1$, illustrating the physical patterns of the modes.

3.2.2. Verification of Efficiency

To assess the efficiency of the present method in free vibration of composite laminates, comparisons of computation time are carried out with the classical FEM. Square laminates with thickness ratio $h/b = 0.1$ and boundary combinations of SSSS and CCCC are considered.

Varying the number of unilateral nodes, the first six nondimensional frequencies are calculated by the present method and the FEM adopting the commonly used Q4 element. It should be pointed out that all the calculations are made by running the same software program on the same computer to guarantee the effectiveness of comparisons. The variations of both the runtime and frequencies in terms of node number per edge are presented in Figures 10 and 11. Note that for clarity, only the variations of the first, third and fifth frequencies are depicted in these figures. One can see that for both CCCC and SSSS cases, when using the present method, only 11 Gauss–Lobatto nodes per edge are needed to make the first six frequency parameters with three decimal digits converge, and the calculation time is less than 0.5 s. In contrast, when using FEM, the first six modes do not converge even when the number of nodes per edge reaches 60, and the

calculation time already exceeds 45 s. These results demonstrates that the present method has incomparable advantages in computation efficiency over the classical FEM, and the remarkable convergence of the current solution is also demonstrated.

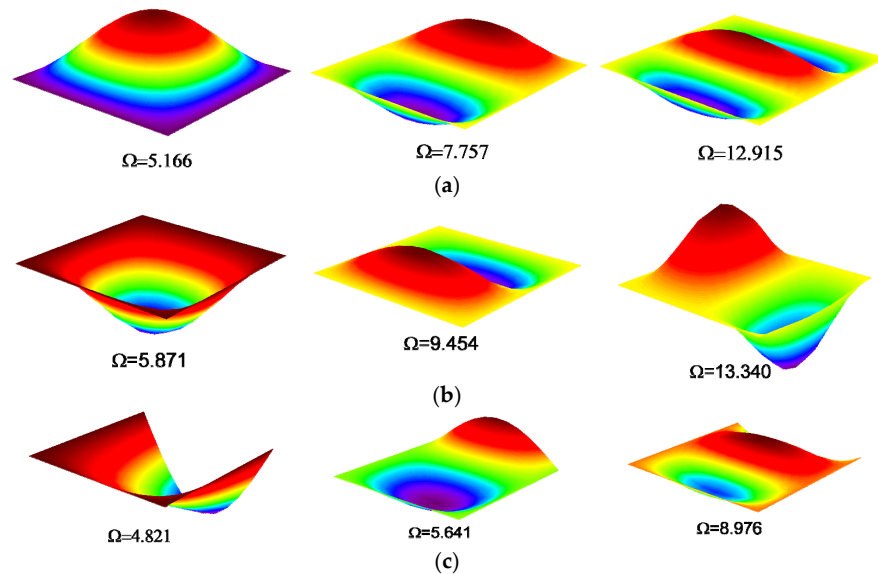


Figure 9. The first three modes for square laminates ($0^\circ, 90^\circ, 0^\circ$) with $h/b = 0.1$: (a) SSSS; (b) SCSC; (c) SSSF.

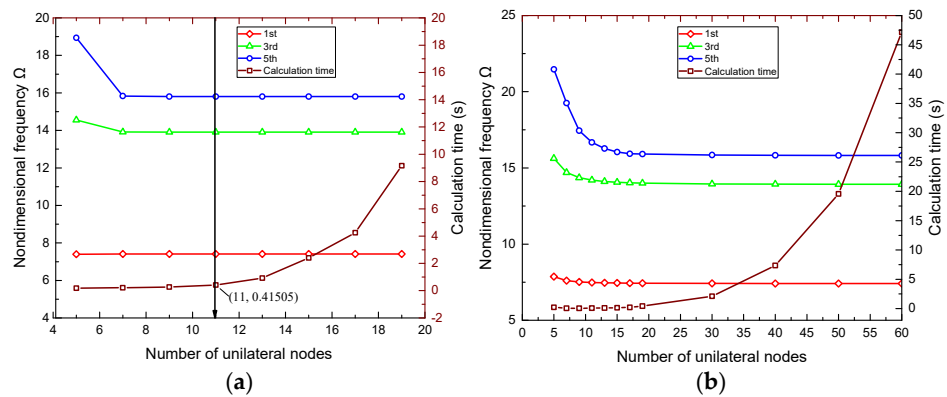


Figure 10. Variations of nondimensional frequencies and the corresponding calculation time vs. The number of unilateral nodes for CCCC laminates with $h/b = 0.1$: (a) the present method; (b) FEM using Q4 element.

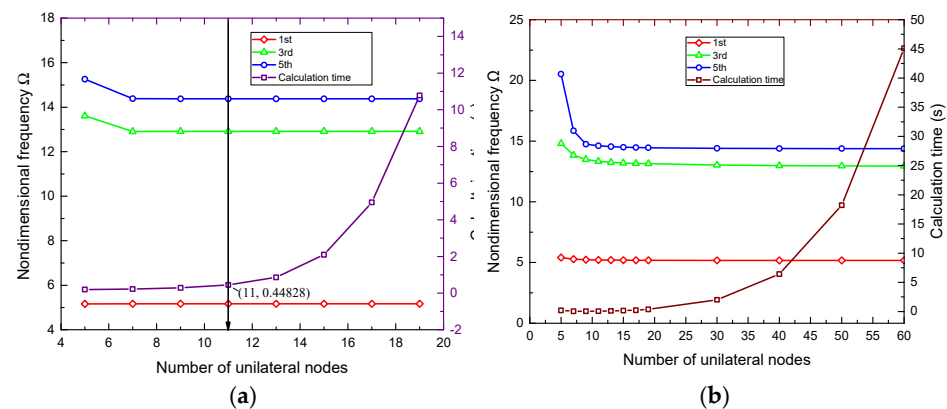


Figure 11. Variations of nondimensional frequencies and the corresponding calculation time vs. The number of unilateral nodes for SSSS laminates with $h/b=0.1$: (a) the present method; (b) FEM using Q4 element.

3.3. Composite Laminates with Elastic Boundary Conditions

The above numerical examples focus on composite laminates with classical boundaries, the free vibration characteristics of which are comprehensive in the published literatures, while those involving arbitrary elastic boundaries are relatively rare. To provide some supplementary and reference results, the following numerical examples are carried out covering three types of elastic boundaries often encountered in practical engineering. The first type referred to as E_1 makes only lateral deflection of plate boundary elastically constrained; two rotations strictly constrained, the corresponding spring stiffness for which is given as: $k_t = 10^2$, $k_{r1} = k_{r2} = 10^8$. Similarly, the second type E_2 allows two rotations elastically restrained with the boundary spring stiffness being set as $k_{r1} = k_{r2} = 10^2$ and $k_t = 10^8$, while in the third type E_3 , both lateral deflection and two rotations are elastically restrained (i.e., $k_t = k_{r1} = k_{r2} = 10^2$).

The non-dimensional frequencies for composite laminates with thickness ratios of 0.01, 0.1, and 0.2 are shown in Table 11. It is shown that the natural frequencies have not changed much for composite laminates with a thin geometry ($h/b = 0.01$) regardless of boundary conditions, which coincide with the conclusions made in the previous analysis. Additionally, one can find that when only the lateral deflection of plate boundary is elastically constrained ($E_1E_1E_1E_1$), the natural frequencies decrease obviously compared to those of the fully clamped laminates, while for the case wherein only two rotations are elastically restrained ($E_2E_2E_2E_2$), there is a slight decline in the natural frequencies, which indicates that constraints on the lateral deflection rather than rotations play a more important role on the natural frequencies for composite laminates with elastic boundaries.

Table 11. The nondimensional frequency Ω for composite laminates with elastic boundary conditions.

Thickness Ratio h/b	B.C.	Order of Frequency					
		1st	2nd	3rd	4th	5th	6th
0.01	CCCC	14.4339	17.3892	24.2667	35.1818	37.7770	39.3875
	$E_1E_1E_1E_1$	14.4271	17.3823	24.2583	35.1684	37.7253	39.3352
	$E_2E_2E_2E_2$	14.4336	17.3890	24.2665	35.1817	37.7762	39.3867
	$E_3E_3E_3E_3$	14.4268	17.3820	24.2581	35.1682	37.7245	39.3344
0.1	CCCC	7.4108	10.3927	13.9129	15.4287	15.8056	19.5720
	$E_1E_1E_1E_1$	6.7022	9.5265	11.9340	13.8435	13.8624	17.2335
	$E_2E_2E_2E_2$	7.3785	10.3671	13.9005	15.4083	15.7924	19.5584
	$E_3E_3E_3E_3$	6.6796	9.5084	11.9316	13.8306	13.8579	17.2287
0.2	CCCC	4.4466	6.6419	7.6996	9.1852	9.7378	11.3991
	$E_1E_1E_1E_1$	3.5877	5.2085	5.9962	7.1819	7.5080	9.0682
	$E_2E_2E_2E_2$	4.4054	6.6109	7.6925	9.1741	9.7175	11.3933
	$E_3E_3E_3E_3$	3.5673	5.1971	5.9838	7.1720	7.5030	9.0614

Although the results presented in this section are for three types of elastic boundary combinations only, the present solution procedure can be readily applied to plates subjected to more complex boundary conditions such as point supports, partial supports, non-uniform elastic restraints, and their combinations.

4. Conclusions

This paper introduces the virtual boundary spring technique into DQFEM to deal with the flexural vibrations of composite laminates. In this new formulated method, boundary conditions are considered in the first step by including the potential energy stored in boundary springs when constructing the energy functional; thus, during the subsequent solution procedures, no special schemes are required to deal with boundary conditions, which is different from the standard DQFEM.

The most significant superiority of the present approach is that it can be universally applicable to composite laminates with any combinations of elastic boundary conditions including all the classical cases without the need of making any change to the solution

procedure. Another advantage of the modified DQFEM over the standard one is that the former facilitates switches of boundary conditions, while in the latter, changing boundary conditions requires researching and eliminating the zero node displacements, which will increase computational cost.

Well-behaved convergence characteristics of the present method are demonstrated. The minimum number of unilateral Gauss–Lobatto nodes to generate convergent solutions and the recommended values of boundary spring stiffnesses are obtained as well. The nondimensional natural frequencies of square laminates under various classical boundary conditions and thickness ratios agree well with available analytical and numerical results from other analyses, which validates the high accuracy of the present method.

Some new results are presented for elastically restrained composite laminates, which can serve as reference values. Moreover, the present solution procedure can be readily extended to composite laminates with more complicated boundary conditions such as multi-point supports, partial supports, non-uniform elastic constraints, and so on.

Author Contributions: Conceptualization, W.X.; methodology, W.X.; software, X.L.; validation, X.L. and L.H.; formal analysis, W.X. and X.L.; writing—original draft preparation, W.X.; writing—review and editing, L.H.; visualization, X.L.; project administration, L.H.; funding acquisition, L.H. All authors have read and agreed to the published version of the manuscript.

Funding: This research was partially supported by the National Natural Science Foundation, China (grant number 51705436), the National Science and Technology Major Project, China (grant number 2017-I-0011-0012), and the Sichuan Province Science and Technology Support Program (grant number 2021JDRC0174).

Institutional Review Board Statement: Not applicable.

Informed Consent Statement: Not applicable.

Data Availability Statement: The data used to support the findings of this study is available from the authors upon request.

Conflicts of Interest: The authors declare no conflict of interest. The funders had no role in the design of the study; in the collection, analyses, or interpretation of data; in the writing of the manuscript; or in the decision to publish the results.

Appendix A

For completeness of the present paper, a brief review of the two-dimensional DQ rule is outlined here. The partial derivatives of $f(x, y)$ can be expressed as the following compact form:

$$\left. \frac{\partial^r f}{\partial x^r} \right|_k = \bar{\mathbf{A}}^{(r)} \bar{\mathbf{f}}, \quad \left. \frac{\partial^s f}{\partial y^s} \right|_k = \bar{\mathbf{B}}^{(s)} \bar{\mathbf{f}}, \quad \left. \frac{\partial^{r+s} f}{\partial x^r \partial y^s} \right|_k = \bar{\mathbf{A}}^{(r)} \bar{\mathbf{B}}^{(s)} \bar{\mathbf{f}}, \quad (\text{A1})$$

where

$$\bar{\mathbf{A}}^{(r)} = \begin{bmatrix} \mathbf{A}^{(r)} & 0 & \cdots & 0 \\ 0 & \mathbf{A}^{(r)} & \cdots & 0 \\ \vdots & \vdots & \ddots & \vdots \\ 0 & 0 & \cdots & \mathbf{A}^{(r)} \end{bmatrix}_{(M \times N) \times (M \times N)}, \quad \mathbf{A}^{(r)} = (A_{ij}^{(r)})_{M \times M'} \quad (\text{A2})$$

$$\bar{\mathbf{B}}^{(s)} = \begin{bmatrix} \mathbf{B}_{11}^{(s)} & \mathbf{B}_{12}^{(s)} & \cdots & \mathbf{B}_{1N}^{(s)} \\ \mathbf{B}_{21}^{(s)} & \mathbf{B}_{22}^{(s)} & \cdots & \mathbf{B}_{2N}^{(s)} \\ \vdots & \vdots & \ddots & \vdots \\ \mathbf{B}_{N1}^{(s)} & \mathbf{B}_{N2}^{(s)} & \cdots & \mathbf{B}_{NN}^{(s)} \end{bmatrix}_{(M \times N) \times (M \times N)}, \quad \mathbf{B}_{ij}^{(s)} = \text{diag}(B_{ij}^{(s)}, \dots, B_{ij}^{(s)})_{M \times M'} \quad (\text{A3})$$

$$\bar{\mathbf{f}} = [f_{11} \quad \cdots \quad f_{M1} \quad f_{12} \quad \cdots \quad f_{M2} \quad \cdots \quad f_{1N} \quad \cdots \quad f_{MN}]^T, \quad (\text{A4})$$

in which M and N represent the number of grid points in the x and y directions, respectively, and $k = (j - 1)M + i$, ($i = 1, 2, \dots, M; j = 1, 2, \dots, N$); $A_{ij}^{(r)}$ and $B_{ij}^{(s)}$ are the weighting coefficients associated with the r th-order partial derivative with respect to x and the s th-order partial derivative with respect to y .

To make the paper self-contained, an overview of the Gauss–Lobatto integration rule is also provided here. The Gauss integration of function $f(x)$ in the interval $[-1, 1]$ with a precision degree of $(2n - 3)$ is given as

$$\int_{-1}^1 f(x)dx = \sum_{j=1}^n C_j f(x_j), \quad (\text{A5})$$

in which the weighting coefficients are given by

$$C_1 = C_n = \frac{2}{n(n-1)}, C_j = \frac{2}{n(n-1)[P_{n-1}(x_j)]^2} (j \neq 1, n), \quad (\text{A6})$$

where x_j is the $(j-1)$ th zero of $P'_{n-1}(x)$, the zeros of which are the eigenvalues of its companion matrix; and the Legendre polynomial $P_n(x)$ of degree n is expressed as

$$P_n(x) = \sum_{k=0}^{\lfloor n/2 \rfloor} \frac{(-1)^k (2n-2k)!}{2^n k! (n-k)! (n-2k)!} x^{n-2k}. \quad (\text{A7})$$

References

1. Sayyad, A.S.; Ghugal, Y.M. On the free vibration analysis of laminated composite and sandwich plates: A review of recent literature with some numerical results. *Compos. Struct.* **2015**, *129*, 177–201. [\[CrossRef\]](#)
2. Akhras, G.; Li, W. Static and free vibration analysis of composite plates using spline finite strips with higher-order shear deformation. *Compos. Part B-Eng.* **2005**, *36*, 496–503. [\[CrossRef\]](#)
3. Carrera, E.; Fazzolari, F.A.; Demasi, L. Vibration analysis of anisotropic simply supported plates by using variable kinematic and Rayleigh-Ritz method. *J. Vib. Acoust.-Trans. ASME* **2011**, *133*, 061017. [\[CrossRef\]](#)
4. Chien, R.-D.; Chen, C.-S. Nonlinear vibration of laminated plates on an elastic foundation. *Thin-Walled Struct.* **2006**, *44*, 852–860. [\[CrossRef\]](#)
5. Gupta, U.S.; Ansari, A.H.; Sharma, S. Buckling and vibration of polar orthotropic circular plate resting on Winkler foundation. *J. Sound Vib.* **2006**, *297*, 457–476. [\[CrossRef\]](#)
6. Kshirsagar, S.; Bhaskar, K. Accurate and elegant free vibration and buckling studies of orthotropic rectangular plates using untruncated infinite series. *J. Sound Vib.* **2008**, *314*, 837–850. [\[CrossRef\]](#)
7. Morozov, E.V.; Lopatin, A.V. Fundamental Frequency of Fully Clamped Composite Sandwich Plate. *J. Sandw. Struct. Mater.* **2010**, *12*, 591–619. [\[CrossRef\]](#)
8. Muthurajan, K.G.; Sankaranarayanan, K.; Tiwari, S.B.; Rao, B.N. Nonlinear vibration analysis of initially stressed thin laminated rectangular plates on elastic foundations. *J. Sound Vib.* **2005**, *282*, 949–969. [\[CrossRef\]](#)
9. Nallim, L.G.; Grossi, R.O. Natural frequencies of symmetrically laminated elliptical and circular plates. *Int. J. Mech. Sci.* **2008**, *50*, 1153–1167. [\[CrossRef\]](#)
10. Ren, X.; Chen, W. Free vibration analysis of laminated and sandwich plates using quadrilateral element based on an improved zig-zag theory. *J. Compos. Mater.* **2011**, *45*, 2173–2187. [\[CrossRef\]](#)
11. Wu, Z.; Chen, W.; Ren, X. An accurate higher-order theory and C-0 finite element for free vibration analysis of laminated composite and sandwich plates. *Compos. Struct.* **2010**, *92*, 1299–1307. [\[CrossRef\]](#)
12. Zhou, D.; Cheung, Y.K.; Au, F.T.K.; Lo, S.H. Three-dimensional vibration analysis of thick rectangular plates using Chebyshev polynomial and Ritz method. *Int. J. Solids Struct.* **2002**, *39*, 6339–6353. [\[CrossRef\]](#)
13. Dai, K.Y.; Liu, G.R.; Lim, K.M.; Chen, X.L. A mesh-free method for static and free vibration analysis of shear deformable laminated composite plates. *J. Sound Vib.* **2004**, *269*, 633–652. [\[CrossRef\]](#)
14. Neves, A.M.A.; Ferreira, A.J.M.; Carrera, E.; Cinefra, M.; Roque, C.M.C.; Jorge, R.M.N.; Soares, C.M.M. Static, free vibration and buckling analysis of isotropic and sandwich functionally graded plates using a quasi-3D higher-order shear deformation theory and a meshless technique. *Compos. Part B-Eng.* **2013**, *44*, 657–674. [\[CrossRef\]](#)
15. Ferreira, A.J.M.; Carrera, E.; Cinefra, M.; Viola, E.; Tornabene, F.; Fantuzzi, N.; Zenkour, A.M. Analysis of thick isotropic and cross-ply laminated plates by generalized differential quadrature method and a Unified Formulation. *Compos. Part B-Eng.* **2014**, *58*, 544–552. [\[CrossRef\]](#)
16. Liew, K.M.; Zhang, J.J.; Ng, T.Y.; Reddy, J.N. Dynamic characteristics of elastic bonding in composite laminates: A free vibration study. *J. Appl. Mech.-Trans. Asme* **2003**, *70*, 860–870. [\[CrossRef\]](#)

17. Xing, Y.; Liu, B. High-accuracy differential quadrature finite element method and its application to free vibrations of thin plate with curvilinear domain. *Int. J. Numer. Methods Eng.* **2009**, *80*, 1718–1742. [[CrossRef](#)]
18. Xing, Y.; Liu, B.; Liu, G. A differential quadrature finite element method. *Int. J. Appl. Mech.* **2010**, *2*, 207–227. [[CrossRef](#)]
19. Du, Y.; Pang, F.; Sun, L.; Li, H. A unified formulation for dynamic behavior analysis of spherical cap with uniform and stepped thickness distribution under different edge constraints. *Thin-Walled Struct.* **2020**, *146*, 106445. [[CrossRef](#)]
20. Kim, K.; Kim, K.; Han, C.; Jang, Y.; Han, P. A method for natural frequency calculation of the functionally graded rectangular plate with general elastic restraints. *AIP Adv.* **2020**, *10*, 085203. [[CrossRef](#)]
21. Kim, K.; Kim, S.; Sok, K.; Pak, C.; Han, K. A modeling method for vibration analysis of cracked beam with arbitrary boundary condition. *J. Ocean. Eng. Sci.* **2018**, *3*, 367–381. [[CrossRef](#)]
22. Wang, Q.; Qin, B.; Shi, D.; Liang, Q. A semi-analytical method for vibration analysis of functionally graded carbon nanotube reinforced composite doubly-curved panels and shells of revolution. *Compos. Struct.* **2017**, *174*, 87–109. [[CrossRef](#)]
23. Wang, Q.; Shao, D.; Qin, B. A simple first-order shear deformation shell theory for vibration analysis of composite laminated open cylindrical shells with general boundary conditions. *Compos. Struct.* **2018**, *184*, 211–232. [[CrossRef](#)]
24. Wang, Q.; Shi, D.; Liang, Q.; Pang, F. Free vibrations of composite laminated doubly-curved shells and panels of revolution with general elastic restraints. *Appl. Math. Modell.* **2017**, *46*, 227–262. [[CrossRef](#)]
25. Wang, Q.; Shi, D.; Liang, Q.; Pang, F. Free vibration of four-parameter functionally graded moderately thick doubly-curved panels and shells of revolution with general boundary conditions. *Appl. Math. Modell.* **2017**, *42*, 705–734. [[CrossRef](#)]
26. Wang, Q.; Shi, D.; Liang, Q.; Shi, X. A unified solution for vibration analysis of functionally graded circular, annular and sector plates with general boundary conditions. *Compos. Part B-Eng.* **2016**, *88*, 264–294. [[CrossRef](#)]
27. Wang, Q.; Shi, D.; Pang, F.; Ahad, F.e. Benchmark solution for free vibration of thick open cylindrical shells on Pasternak foundation with general boundary conditions. *Meccanica* **2017**, *52*, 457–482. [[CrossRef](#)]
28. Wang, Q.; Shi, D.; Shi, X. A modified solution for the free vibration analysis of moderately thick orthotropic rectangular plates with general boundary conditions, internal line supports and resting on elastic foundation. *Meccanica* **2016**, *51*, 1985–2017. [[CrossRef](#)]
29. Mindlin, R.D. Influence of Rotatory Inertia and Shear on Flexural Motions of Isotropic, Elastic Plates. *J. Appl. Mech.* **1951**, *18*, 31–38. [[CrossRef](#)]
30. Reissner, E. The Effect of Transverse Shear Deformation on the Bending of Elastic Plates. *J. Appl. Mech.* **1945**, *12*, A69–A77. [[CrossRef](#)]
31. Bert, C.W.; Malik, M. Free vibration analysis of thin cylindrical shells by the differential quadrature method. *J. Press. Vessel Technol.* **1996**, *118*, 1–12. [[CrossRef](#)]
32. Bert, C.W.; Malik, M. The differential quadrature method for irregular domains and application to plate vibration. *Int. J. Mech. Sci.* **1996**, *38*, 589–606. [[CrossRef](#)]
33. Malik, M.; Bert, C. Implementing multiple boundary conditions in the DQ solution of higher-order PDEs: Application to free vibration of plates. *Int. J. Numer. Methods Eng.* **1996**, *39*, 1237–1258. [[CrossRef](#)]
34. Liu, B.; Xing, Y.F.; Reddy, J.N. Exact compact characteristic equations and new results for free vibrations of orthotropic rectangular Mindlin plates. *Compos. Struct.* **2014**, *118*, 316–321. [[CrossRef](#)]
35. Liew, K.M. Solving the vibration of thick symmetric laminates by Reissner/Mindlin plate theory and the p-Ritz method. *J. Sound Vib.* **1996**, *198*, 343–360. [[CrossRef](#)]